NANOSYSTEMS: PHYSICS, CHEMISTRY, MATHEMATICS, 2018, 9 (3), P. 378–388

Phase composition and photoluminescence correlations in nanocrystalline ZrO_2:Eu^{3+} phosphors synthesized under hydrothermal conditions

A. N. Bugrov[1,2], R. Yu. Smyslov[1,3], A. Yu. Zavialova[2,4], D. A. Kirilenko[5,6], D. V. Pankin[7]

[1]Institute of macromolecular compounds RAS, Bolshoy pr. 31, 199004, St. Petersburg, Russia
[2]Saint Petersburg Electrotechnical University "LETI", ul. Professora Popova 5, 197376, St. Petersburg, Russia
[3]Petersburg Nuclear Physics Institute, NRC KI, Orlova roscha mcr. 1, 188300, Gatchina, Leningrad region, Russia
[4]Saint Petersburg State Institute of Technology (Technical University), Moskovsky pr. 26, 190013, St. Petersburg, Russia
[5]Ioffe Institute RAS, Politekhnicheskaya ul. 26, 194021, St. Petersburg, Russia
[6]ITMO University, Kronverskii av. 49, 197101, St. Petersburg, Russia
[7]Research park SPbU, Ulianovskaya 5, 198504, St. Petersburg, Russia

alexander.n.bugrov@gmail.com

PACS 78.67. n; 78.67.Bf **DOI 10.17586/2220-8054-2018-9-3-378-388**

Luminescent zirconia nanoparticles with europium ion content 1 and 10 mol.% were synthesized under hydrothermal conditions. Annealing of ZrO_2: 1 mol. Eu^{3+} nanoparticles made it possible to obtain a sample with a high monoclinic phase content up to 92 %. An increase in the concentration of Eu^{3+} ions introduced into the zirconia crystal lattice has made it possible to almost completely convert its monoclinic and tetragonal phases into cubic modification. The phase composition of the synthesized samples was determined by powder X-ray diffraction, electron microdiffraction, and Raman spectroscopy. Analysis of the crystallographic data and the luminescent spectra helped to reveal correlations between the ZrO_2:Eu^{3+} nanophosphor structure and the energy redistribution of Eu^{3+} optical transitions at 614 – 626 nm and 606 – 633 nm wavelengths. In addition, a relationship was established between the phase composition of nanoparticles based on zirconia and the luminescence lifetime of Eu^{3+} ions.

Keywords: hydrothermal synthesis, solid solutions, zirconia, europium, phase transitions, nanoparticles, photoluminescence, fluorescence lifetime.

Received: 4 April 2018

Revised: 14 April 2018

1. Introduction

Zirconia and its solid solutions have some non-trivial physico-chemical properties. It is worth mentioning mechanical strength [1,2], hardness [3,4], wear and crack resistance [5,6], high thermal expansion [7], low thermal conductivity [8], and photocatalytic activity [9]. Zirconia transparency is in a broad spectral range from mid-wavelength IR ($\lambda < 8$ μm) to near UV ($\lambda > 300$ nm) [10]. Chemical and photochemical stability [11, 12], along with a high refractive index [13], low phonon energy [14] and large band gap [15] make zirconia an ideal matrix for obtaining highly effective luminescent materials [16].

Zirconia is found in the form of three main polymorphic modifications. A thermodynamically stable monoclinic modification of zirconia (*m*-ZrO_2) occurs naturally in the form of baddeleyite minerals. Monoclinic (α) zirconia P21/c [17] exists at room temperature and up to 1170 °C; above this temperature, its transition into a denser tetragonal (β) form occurs. The tetragonal phase P42/nmc [18] is stable in the temperature range 1170 – 2370 °C, whose upper limit determines the formation of the cubic (γ) modification of ZrO_2 belonging to the structural type of fluorite Fm3m [19].

The highest performance indicators have metastable high-temperature modifications of ZrO_2 (cubic and tetragonal), which are stabilized by the introduction of Mg, Ca, Sc and rare earth elements (REE) ions. Substitutional solid solutions based on zirconia are obtained by introducing the trivalent ions of II and III groups in the periodic system or REE ions (in particular lanthanides) into the ZrO_2 crystal lattice [20–23].

Oxygen vacancies play a significant role in the formation of the tetragonal and cubic phases of zirconia. Phase stabilization using only oxygen vacancies was confirmed by theoretical calculations [24]. In addition to phase stabilization, oxygen vacancies also strongly affect the luminescence intensity of the Ln^{3+} ions and the Stark splitting of the spectral terms [25, 26]. The change in the luminescence intensity and the phase transition from ZrO_2 equilibrium modification to metastable tetragonal and even cubic occurs with an increase of the lanthanide content in its crystal lattice. For stabilizing the tetragonal phase, it is usually necessary to add up to 6 mol.% of the

trivalent ions, whereas the required concentration to achieve the cubic phase is 10 – 12 mol.% [27]. The tetragonal with or separately from the monoclinic phase of ZrO_2 are formed depending on the synthesis method at a low concentration of Ln^{3+} ions. High annealing temperatures lead to the formation of large grains, thereby reducing the effect of surface defects on nonradiative recombination of excitations. Both defects (volume and surface defects) and structure have a significant effect on the intensity of luminescence [28].

Lanthanide ions are widely used as local probes to identify the crystalline structure of materials. The trivalent europium ion is well known as a red-emitting activator due to its $^5D_0$–^7F_j ($j = 0, 1, 2, 3, 4$). These transitions are very sensitive to structural changes and depend on the local symmetry of the crystal field around the Eu^{3+} ions in different oxide matrix [29]. Europium is preferable as a luminescent structural probe for determining the number, location, and symmetry of the metal ions in the compound, as well as the population of their levels because of its non-degenerate emission state $^5D_0$. Other lanthanide ions have transitions, which are usually a mixture of magnetic (MDT, $^5D_0$–$^7F_1$) and dielectric (EDT, $^5D_0$–$^7F_2$) dipole transitions, and the symmetry effects in them are less pronounced [30].

Today in the literature there are several papers on the luminescence of zirconia nanoparticles doped with europium ions [31–35]. They provide information on changes in the splitting of EDT and MDT for Eu^{3+} ions in various crystal structures of ZrO_2. Moreover, the researchers consider aspects of the crystal structure effect of zirconia on the luminescence lifetime of Eu^{3+} ions in order to increase the productivity of optical devices based on them. It is critical from a fundamental point of view to identify correlations between the zirconia crystalline structure and the europium luminescence properties in the ZrO_2:Eu^{3+} nanoparticles, and also the nature of their changes as a function of temperature and dopant concentration. Also, the combination of the physico-chemical properties of ZrO_2 matrix acting as an oscillator with the europium optical characteristics gives a considerable potential in the field of photonic applications, such as solid-state lasers, sensors, optical amplifiers, scintillators, phosphors and lamps [36].

In this regard, this work aimed to obtain ZrO_2:Eu^{3+} nanoparticles under hydrothermal conditions and to vary their phase composition due to annealing at high temperature, as well as changing the lanthanide concentration in the zirconia lattice with subsequent analysis of the structure influence on the europium luminescent properties.

2. Experimental methods

The compositions with 1 and 10 mol.% of europium ions which make it possible to obtain zirconia mainly in tetragonal and cubic polymorphous modifications were selected for the synthesis of luminescent nanoparticles according to the ZrO_2–Eu_2O_3 phase diagram [37]. ZrO_2:Eu^{3+} nanoparticles were synthesized by coprecipitation of zirconium and europium hydroxides from 0.5 M chloride solutions, followed by dehydration of the resulting mixtures under hydrothermal conditions. Coprecipitation of hydroxides was performed using NH_4OH solution (25 %) at room temperature and continuous mechanical stirring to pH = 8. The resulting white precipitates were washed with distilled water until a negative reaction to chloride ions and neutral pH, using the decantation method. Then, the $ZrO(OH)_2$–$Eu(OH)_3$ compositions were dried in air at 100 °C. Hydrothermal treatment of coprecipitated hydroxides was performed in steel autoclaves according to the procedure given in [38].

Wide angle X-ray diffraction analysis of synthesized nanoparticles and annealed samples were obtained at scattering angles varying from 10 ° to 100 ° with 0.02 ° step using a Rigaku SmartLab diffractometer (Tokyo, Japan). Cu-$K\alpha$ radiation (40 kV, 40 mA) was used. The identification of ZrO_2 crystalline phases was performed in Crystallographica Search-Match software by comparing our experimental data with powder diffraction files from the ICDD (International Centre for Diffraction Data) database. The crystallite size was estimated from the broadening of X-ray diffraction (XRD) lines of the ZrO_2:Eu^{3+} nanopowders in the PD-Win 4.0 program complex using the Scherrer formula. The ReX software [39] with the Crystallography Open Database (COD) was used for quantitative X-ray phase analysis and calculation of lattice parameters from WAXD data.

The size, shape and phase composition of the ZrO_2:Eu^{3+} nanoparticles were determined using a transmission electron microscope JEM-2100F (JEOL microscope, Tokyo, Japan) at an acceleration voltage of 90 kV. Bright-field images and electron diffraction patterns were obtained. Sample preparation included dispersing of ZrO_2:Eu^{3+} nanoparticles in ethanol by ultrasonic bath and subsequent dipping of the graphene foil grids in the resulting slurry.

Raman measurements were performed using LabRAM HR800 (Horiba Jobin Yvon, Japan) with 1800 gr/mm diffraction grade in backscattering geometry. Raman spectra were recorded with excitation by a 488 nm of Ar^+ laser. Before measurement, the spectrometer was calibrated using 520.7 cm^{-1} line of silicon standard.

The elemental composition of nanoparticles was controlled by the microanalysis system INCA (Oxford Instruments, UK) using a Zeiss SUPRA 55VP field-emission from Carl Zeiss AG (Germany).

The emission spectra and the luminescence lifetime of ZrO_2:Eu^{3+} nanoparticles were recorded with a spectrophotometer LS-100 BASE (PTI Lasers INC, Canada). The geometric width of the output slit of the excitation

monochromator was 1.25 mm, and that of the entrance slit of the fluorescence monochromator was 0.5 mm. The wavelength interval for the emission spectra of nanophosphors was set at 560 – 770 nm, and photoluminescence was excited in the range of 205 – 315 nm. The xenon lamp in the pulsed mode was used as a source of excitation. The integration window of the signal was 100 – 2000 μs.

The luminescence lifetimes for nanophosphors containing Eu^{3+} were determined from the emission intensity decay using pulse xenon lamp mode. The luminescence was excited at 247 nm, and it was observed at 606 and 614 nm. The values of lifetimes were calculated with an iterative fitting procedure using QtiPlot software [40]. The reliability of coincidence of the experimental signal with that calculated was monitored by the statistical parameter χ_2, which characterizes the extent to which the experimental data coincide with the theoretical model.

3. Results and discussion

A mixture of coprecipitated zirconium and europium hydroxides prepared for the synthesis of ZrO_2:1 mol.% Eu^{3+} nanoparticlesis amorphous according to XRD data. Its hydrothermal treatment over 4 hours at 250 °C and 15 MPa led to the formation of ZrO_2:Eu^{3+} nanocrystals with an average size of 15 ± 3 nm consisting of monoclinic and tetragonal polymorphous modifications in the 22:78 ratio (Fig. 1(a)). ZrO_2:1 mol.% Eu^{3+} nanoparticles were annealed in air at 1200 °C for 2 hours and slowly cooled to room temperature together with the furnace in order to increase the monoclinic phase content. During the heating process at the temperature of the equilibrium phase transition ($T = 1170$ °C), the existing monoclinic zirconia (*m*-ZrO_2) transforms into a tetragonal polymorphic modification. Since this phase transition is reversible, zirconia is transformed into an equilibrium modification *m*-ZrO_2 with slow cooling. The quantitative X-ray phase analysis performed in the ReX program using the cards of the diffraction standards for monoclinic [41] and tetragonal [42] zirconia showed that phase ratio is 92:8 after annealing of ZrO_2:1 mol.% Eu^{3+} nanoparticles (Fig. 1(b)). The Eu^{3+} ions introduced into the crystal lattice of zirconia nanoparticles stabilize the metastable tetragonal phase (*t*-ZrO_2) and do not entirely transfer it to equilibrium upon cooling. The average crystallite size calculated from the broadening of the X-ray diffraction maxima for both the monoclinic and tetragonal phases after annealing was 29 ± 5 nm. Eu^{3+} ions in an amount of 10 mol.% were introduced into the zirconia crystalline structure to stabilize its cubic phase (*c*-ZrO_2) and reduce the monoclinic content to a minimum. In this case, the ZrO_2:10 mol.% Eu^{3+} nanoparticles consisted of 98 % of the zirconia cubic phase, and the remaining 2 vol.% corresponded to its monoclinic polymorphic modification (Fig. 1(c)). *c*-ZrO_2 [43] and *m*-ZrO_2 cards [41] from the COD database were used to calculate the phase composition of nanoparticles. The size of the coherent scattering regions for ZrO_2:10 mol.% Eu^{3+} nanoparticles, calculated from the Scherrer equation, was 12 ± 2 nm. The portions of *m*-, *t*-, and *c*-ZrO_2 phases, calculated using intensities of Raman shifts, are correlated with those obtained with Rietveld refinement (Table 1). The parameters of the unit cell for the monoclinic, tetragonal, and cubic phases refined by the Rietveld method from X-ray diffractograms of ZrO_2:Eu^{3+} nanoparticles (Table 1) are comparable with the literature data [44].

TABLE 1. Structural parameters of ZrO_2:Eu^{3+} nanoparticles

Sample	Phase composition	Unit cell parameters	$\frac{I_{m/(t,c)}}{I_m + I_{t,c}}$ [1)]
ZrO_2:1 mol.% Eu^{3+}	22 vol.% m-ZrO_2	–	0.209
	78 vol.% t-ZrO_2	$a = 3.6102$; $b = 3.6102$; $c = 5.1847$ $\alpha = 90$ °; $\beta = 90$ °; $\gamma = 90$ °	0.791
ZrO_2:1 mol.% Eu^{3+} (annealing 1200 °C)	92 vol.% m-ZrO_2	$a = 5.1575$; $b = 5.2055$; $c = 5.3115$ $\alpha = 90$ °; $\beta = 99.03$ °; $\gamma = 90$ °	0.867
	8 vol.% t-ZrO_2	$a = 3.6003$; $b = 3.6003$; $c = 5.1787$ $\alpha = 90$ °; $\beta = 90$ °; $\gamma = 90$ °	0.133
ZrO_2:10 mol.% Eu^{3+}	2 vol.% m-ZrO_2	–	0.114
	98 vol.% c-ZrO_2	$a = 5.1548$; $b = 5.1548$; $c = 5.1548$ $\alpha = 90$ °; $\beta = 90$ °; $\gamma = 90$ °	–

Note: [1)]Portions of *m*-, *t*-, and *c*-ZrO_2 phases were calculated using intensities of Raman shifts I_m, at 177.7 cm^{-1} and $I_{t,c}$ at 146 cm^{-1} in Fig. 4.

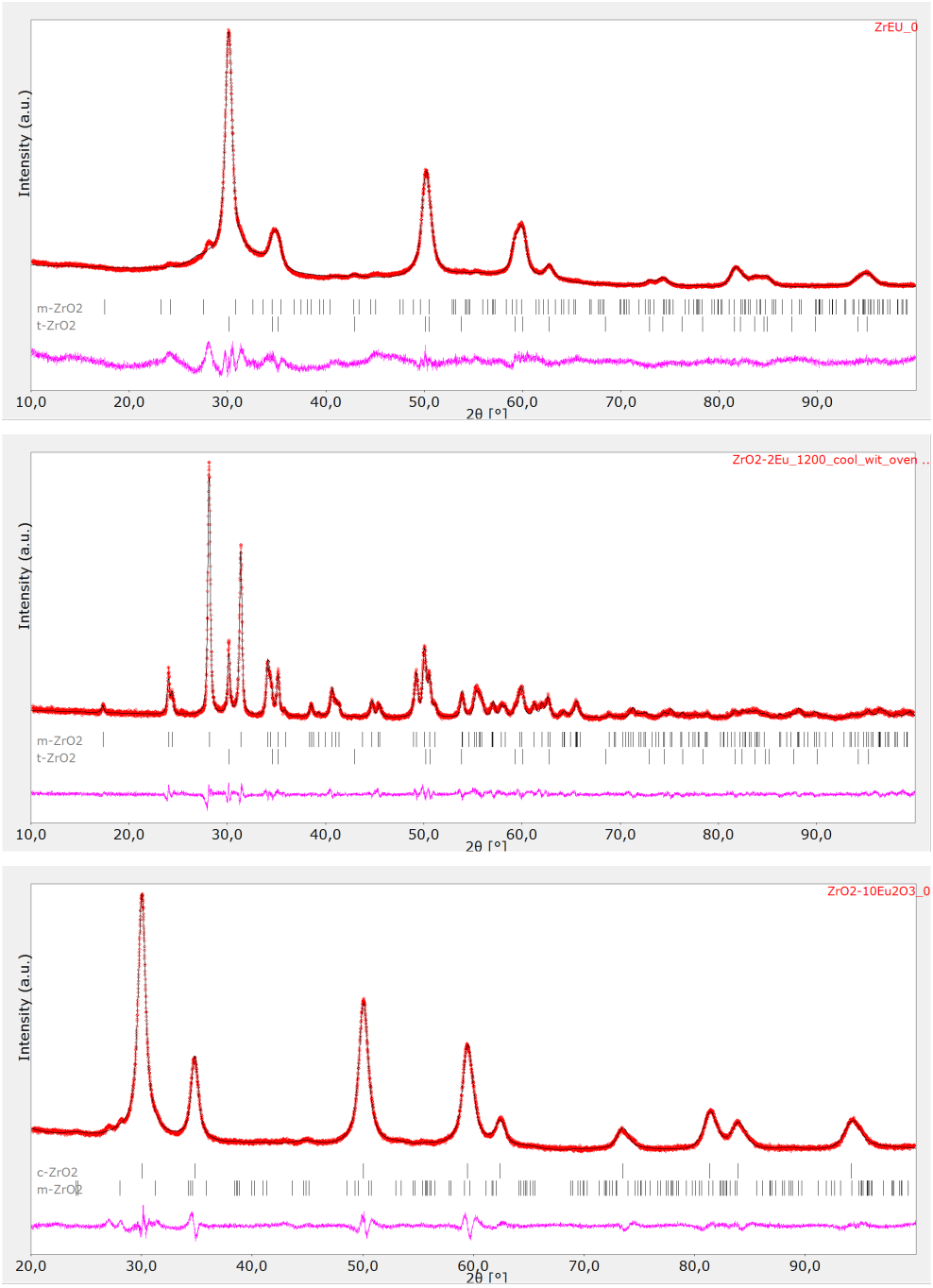

FIG. 1. Line profile analysis in the Rietveld method of powder X-ray diffractograms for nanoparticles: a – ZrO_2: 1 mol.% Eu^{3+}; b – ZrO_2: 1 mol.% Eu^{3+} annealed at 1200 °C; c – ZrO_2: 10 mol.% Eu^{3+}

The diameter of the ZrO_2:1 mol.% Eu^{3+} nanoparticles from the TEM micrographs (Fig. 2(1a)) correlates with the average crystallite size calculated from the X-ray diffractogram (Fig. 1a). Annealing the sample at 1200 °C leads to the fusion of nanocrystals to submicron dimensions (Fig. 2(1b)). In the case of zirconia stabilized with 10 mol.% europium ions, microphotographs contain both spherical particles 10 nm in diameter and cubical with an average size of 13 nm (Fig. 2(1c)). According to electron microdiffraction data, the ZrO_2:1 mol.% Eu^{3+} nanoparticles in native form and after thermal treatment contain the monoclinic and tetragonal phases (Fig. 2(2a,2b)), and with the increase in the concentration of europium ions only the fluorite-like structure stabilizes (Fig. 2(2c)).

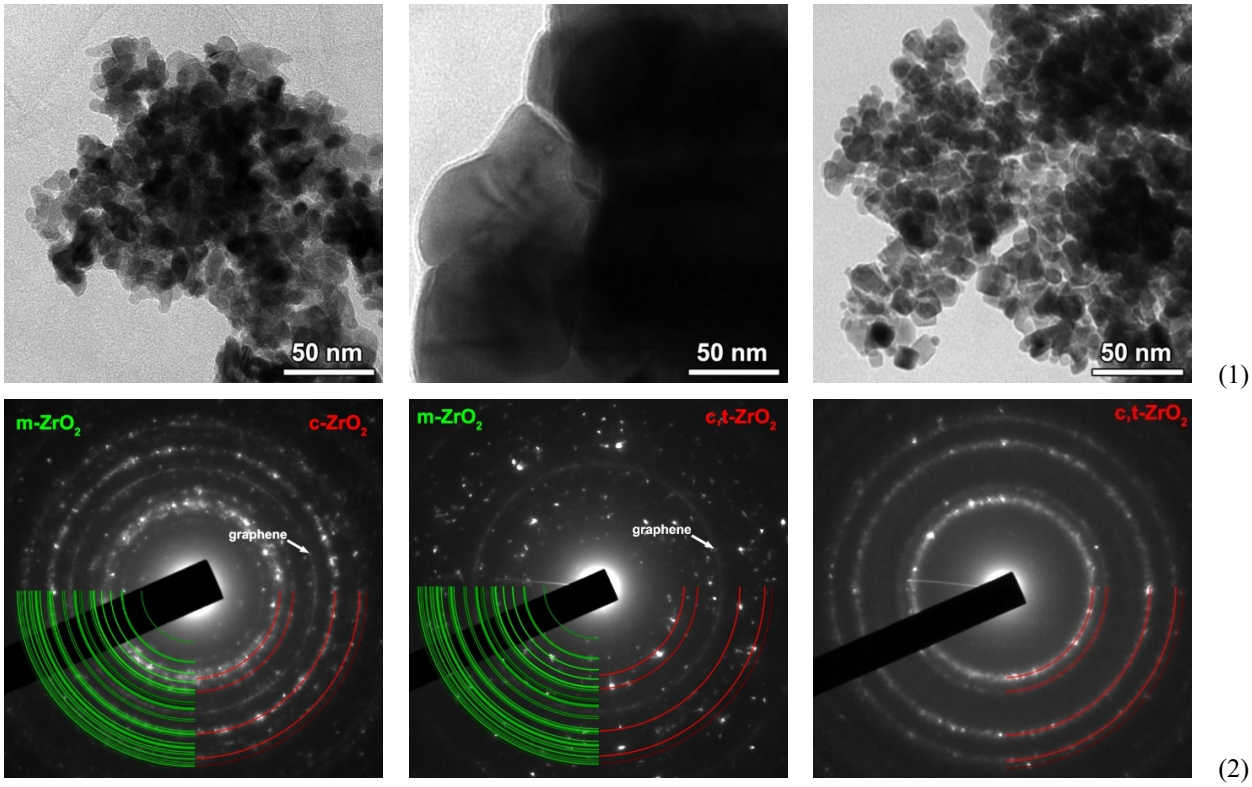

FIG. 2. TEM micrographs (1) and electronic diffraction patterns (2) of nanoparticles: a – ZrO_2:1 mol.% Eu^{3+}; b – ZrO_2:1 mol.% Eu^{3+} annealed at 1200 °C; c – ZrO_2:10 mol.% Eu^{3+}

The data of the Energy Dispersive X-ray Spectrometry (EDS) analysis, shown in Fig. 3 and Table 2, confirm the compliance of europium content (mol.%) in ZrO_2-based nanophosphors to the values determined by synthesis.

TABLE 2. EDS analysis of ZrO_2:Eu^{3+} nanoparticles

Sample	Zr	Eu	O
	wt.%		
ZrO_2:1 mol.% Eu^{3+}	67.2 ± 0.9	1.6 ± 0.5	31.2 ± 0.8
ZrO_2:10 mol.% Eu^{3+}	61.9 ± 0.9	12.1 ± 0.5	26 ± 0.8

The differences between *t-*, *c*-ZrO_2 and *m*-ZrO_2 phases are reflected in the normalized Raman spectra (Fig. 4). For the nanoparticles with 1 mol% Eu^{3+} subjected to subsequent annealing at 1200 °C, the Raman shifts indicate that the sample preferably consists of the *m*-ZrO_2 phase (curve 1). The strong peaks are at 183, 335, and 474 cm^{-1} [45, 46]. Besides, the small number of bands observed for the sample with 1 mol.% Eu^{3+} allows identifying the *t*-ZrO_2 phase considerably easily with the peaks shown at 149, 224, 292, 324, 407, 456, and 636 cm^{-1} (curve 2) [47]. In the Raman spectra of ZrO_2:10 mol.% Eu^{3+} nanoparticles, there are mainly hard-to-separate bands of the high-temperature metastable *c*-zirconia phases with a narrow band at 145 cm^{-1} and broad bands 230 – 290 cm^{-1}, 400 – 430 cm^{-1}, 530 – 670 cm^{-1} and a shoulder at 301 cm^{-1} (curve 3) [48]. Some peaks of the monoclinic modification are likely to appear at this. The phase ratio in the samples of ZrO_2:Eu^{3+}nanoparticles, calculated from the Raman spectra, correlates with the XRD data refined by the Rietveld method (Table 1).

Figure 5 shows the photoluminescence spectra of nanophosphors containing Eu^{3+} ions in the ZrO_2 matrix for the three cases studied. The emission band represents a quasilinear spectrum and consists of characteristic

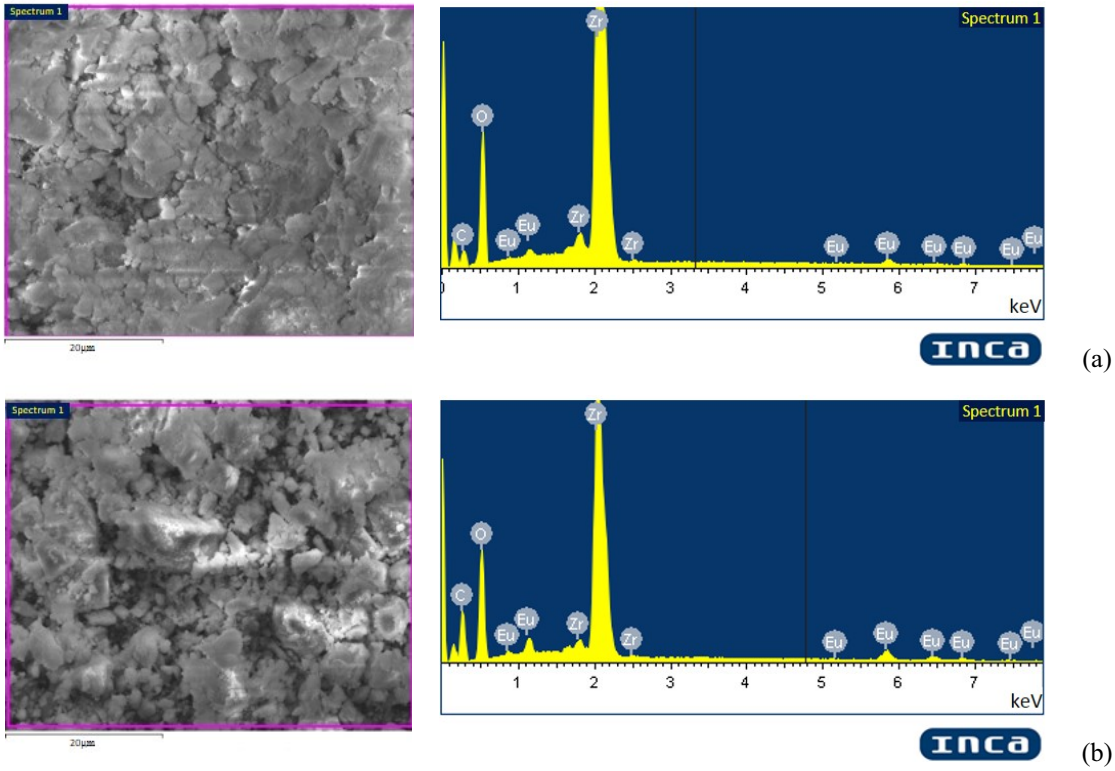

FIG. 3. SEM selected area image and EDS spectrum of ZrO_2 nanoparticles with 1 mol.% (a) and 10 mol.% Eu^{3+} (b)

luminescence peaks corresponding to optical transitions between the spectral terms of the ion Eu^{3+}: $^5D_0 \rightarrow ^7F_J$ ($0 \leq J \leq 6$) 581, 592, 614, 655 and 712 nm [49]. The optical transition of $^5D_0 \rightarrow ^7F_2$ splits into 4 peaks in a zirconia crystal field with maxima at 606, 614, 625, 633 nm and different contributions, depending on the ratio of ZrO_2 polymorphous modifications. The more significant is a less symmetrical *m*-phase as compared with *t*- or *c*-ZrO_2 phases, the higher is the contribution of the peak at 614 nm compared to the peak at 606 nm (compare curve 1 with curves 2 and 3). In the optical transition $^5D_0 \rightarrow ^7F_4$, it is also seen that the higher symmetry of the prevailing phase is, the stronger the Stark effect is, i.e., this peak is more shifted into the long-wavelength region. So, the maximum for the *m*-phase is at 712 nm, for *t*- or *c*-ZrO_2 it is already at 715.3 nm.

Figure 6 shows the luminescence intensity decays $I_{lum}(t)$ of Eu^{3+} in the ZrO_2 matrix. The table includes the calculated parameters of the curves using the stretched exponential function first used by A. Werner in 1907 to describe the complex luminescence decay, and then by Theodor Förster in 1949 to describe the fluorescence decay of electron energy donors [50–52]:

$$I_{lum}(t) = I_{lum}(0) \exp\left[-\left(\frac{t - t_0}{\tau_{PL}}\right)^{\beta}\right], \tag{1}$$

where t is decay time; $I_{lum}(0)$ is the luminescence intensity at $t = 0$; τ_{PL} is the photoluminescence lifetime; t_0 is the time shift in the observation channels; β is the width of luminescence lifetime spectrum in the excited states ($0 \leq \beta \leq 1$).

Analysis of the luminescence decay data for the three studied systems showed (Table 3) that the more homogeneous system regarding the polymorphic modification content (*m*-phase of ZrO_2) is, the narrower lifetime spectrum range of the excited state, characterized by the value $D_f = 2 - \beta$, we observe [52–54]. The less symmetrical *m*-phase has the shortest luminescence lifetime – 0.57 ms, versus 2.39 ms for the *t*-ZrO_2. The decrease in the luminescence lifetime for nanoparticles with a stabilized cubic phase of zirconia (10 mol% Eu^{3+}), in comparison with the ZrO_2:1 mol.% Eu^{3+} sample which contains a mixture of *m*/*t*-phases may indicate the occurrence of concentration quenching at a high europium concentration.

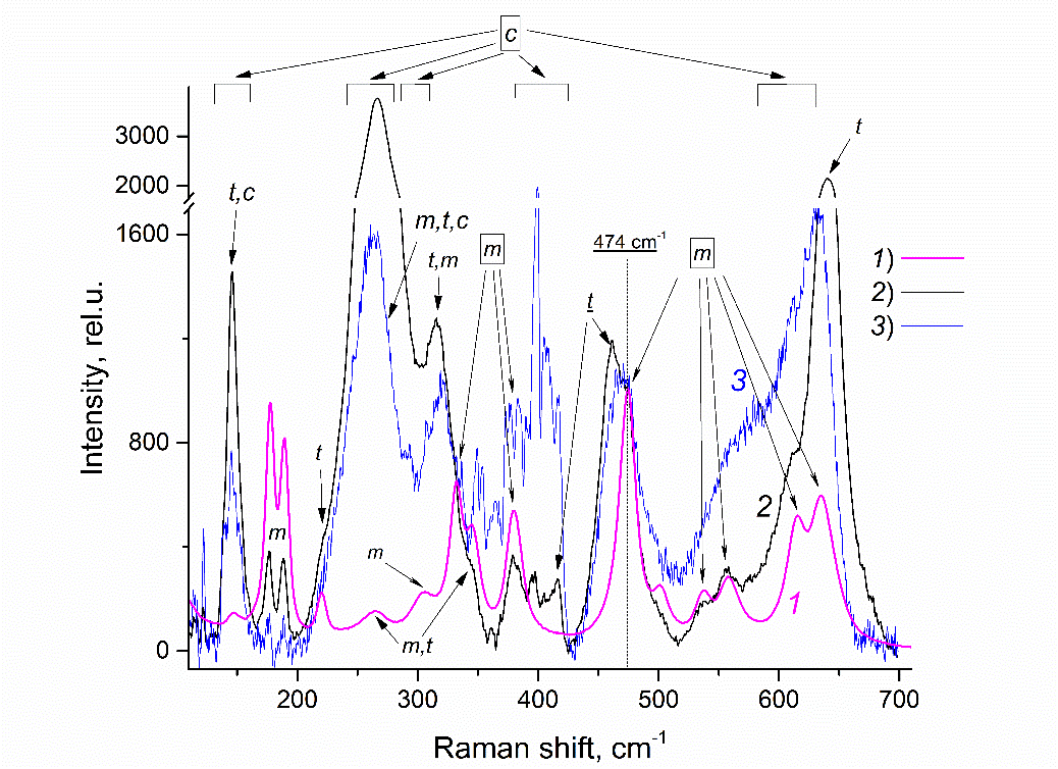

FIG. 4. Normalized Raman spectra of nanoparticles: 1 – ZrO_2:1 mol.% Eu^{3+} annealed at 1200 °C; 2 – ZrO_2:1 mol.% Eu^{3+}; 3 – ZrO_2:10 mol.% Eu^{3+}. Spectra were normalized at 474 cm^{-1}

TABLE 3. Analysis of the luminescence decay for ZrO_2:Eu^{3+} nanoparticles

No.	Sample	Phase composition, mol.%			τ_{PL}, ms	β	$D_f = 2 - \beta$	$I_{lum}(0)$	$\chi^2_{red.}$
		m	t	c					
1	ZrO_2:1 mol.% Eu^{3+} (annealing 1200 °C)	92	8	–	0.57±0.02	0.898(12)	1.102	318.0±35.2	2.08
2	ZrO_2:1 mol.% Eu^{3+}	22	78	–	2.39±0.03	0.872(7)	1.128	188.6±1.7	1.84
3	ZrO_2:10 mol.% Eu^{3+}	2	–	98	1.18±0.01	0.749(5)	1.251	187.1±1.1	1.28

Note: the luminescence decay was observed at 606 nm for ZrO_2 nanoparticles with 1 and 10 mol.% Eu^{3+} and at 614 nm for the annealed sample using the excitation wavelength of 247 nm.

4. Conclusions

The ZrO_2:1 mol.% Eu^{3+} nanophosphors represented by a mixture of monoclinic and tetragonal phases with a set of interconfiguration $4f^{n-1}5d$-$4f^n$ optical transitions in the red region of the emission spectrum, and quasilinear bands distinctive for europium ions were obtained under hydrothermal conditions. Samples, where europium ions were predominantly in the crystal lattice of either the metastable or the equilibrium zirconia phase, were obtained by increasing the concentration of the stabilizer ions to 10 mol.% and annealing the synthesized nanoparticles at a temperature of 1200 °C. It was shown that the luminescent properties of Eu^{3+} ions in the zirconia crystal lattice are very sensitive to the phase composition of the nanoparticles. The Stark splitting of the dielectric ($^5D_0 \rightarrow {}^7F_1$) and magnetic ($^5D_0 \rightarrow {}^7F_1$) dipole transitions of Eu^{3+} ions with maxima at 590 and 606 nm is observed for ZrO_2 cubic phase with a more symmetric structure. The contribution of the peaks at 596 and 614 nm significantly

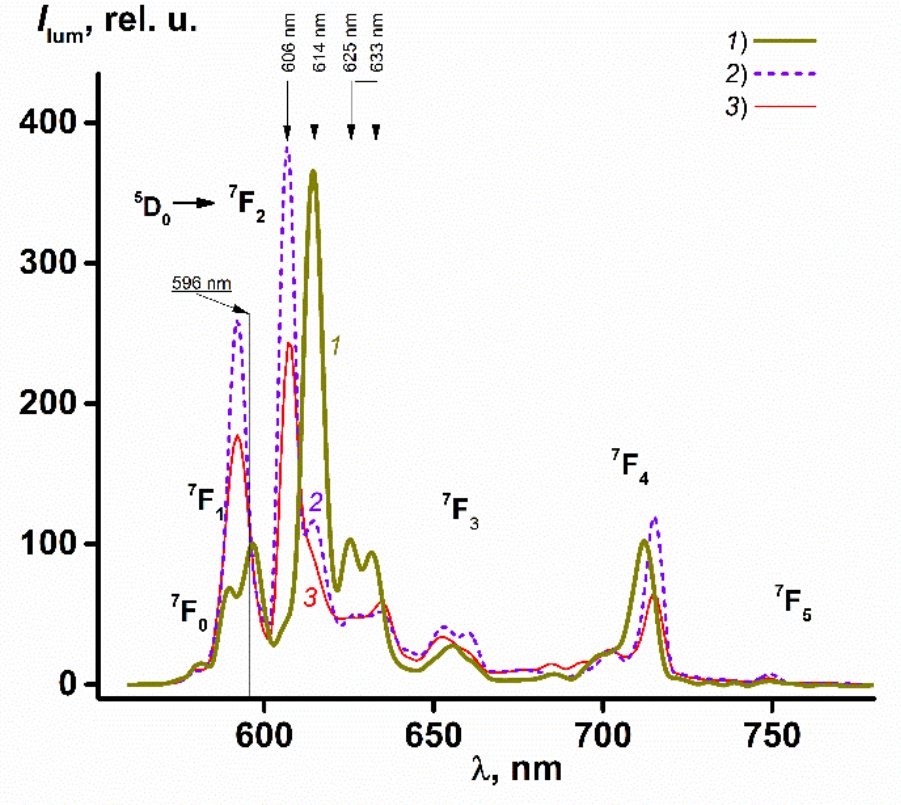

FIG. 5. Normalized luminescence spectra of nanoparticles: 1 – ZrO_2:1 mol.% Eu^{3+} annealed at 1200 °C; 2 – ZrO_2:1 mol.% Eu^{3+}; 3 – ZrO_2:10 mol.% Eu^{3+}. Excitation is at 247 nm. Photoluminescence spectra are normalized at 596 nm

increases in the case of a sample in which the zirconia monoclinic modification predominates. The luminescence lifetime of Eu^{3+} ions also correlates with the symmetry of the crystal field, a more extended 2.39 ms refers to *t*-ZrO_2, and a short 0.57 ms is characteristic of the monoclinic phase. Thus, Eu^{3+} ions, given their sensitivity to the environment, can be used as a structural probe, and the method of luminescence spectroscopy serves to identify the phase composition of the oscillator matrix.

Acknowledgements

Dr. A. N. Bugrov thanks the Russian Foundation for Basic Research (grant number 16-33-60227) for financial support. The work was performed with the use of the equipment of the Joint Research Center "Material science and characterization in advanced technology" (Ioffe Institute, St. Petersburg, Russia). The experimental work was facilitated by the Engineering Center equipment of the St. Petersburg State Technological Institute (Technical University). The Raman spectrum measurements were performed at the Center for Optical and Laser Materials Research, St. Petersburg State University.

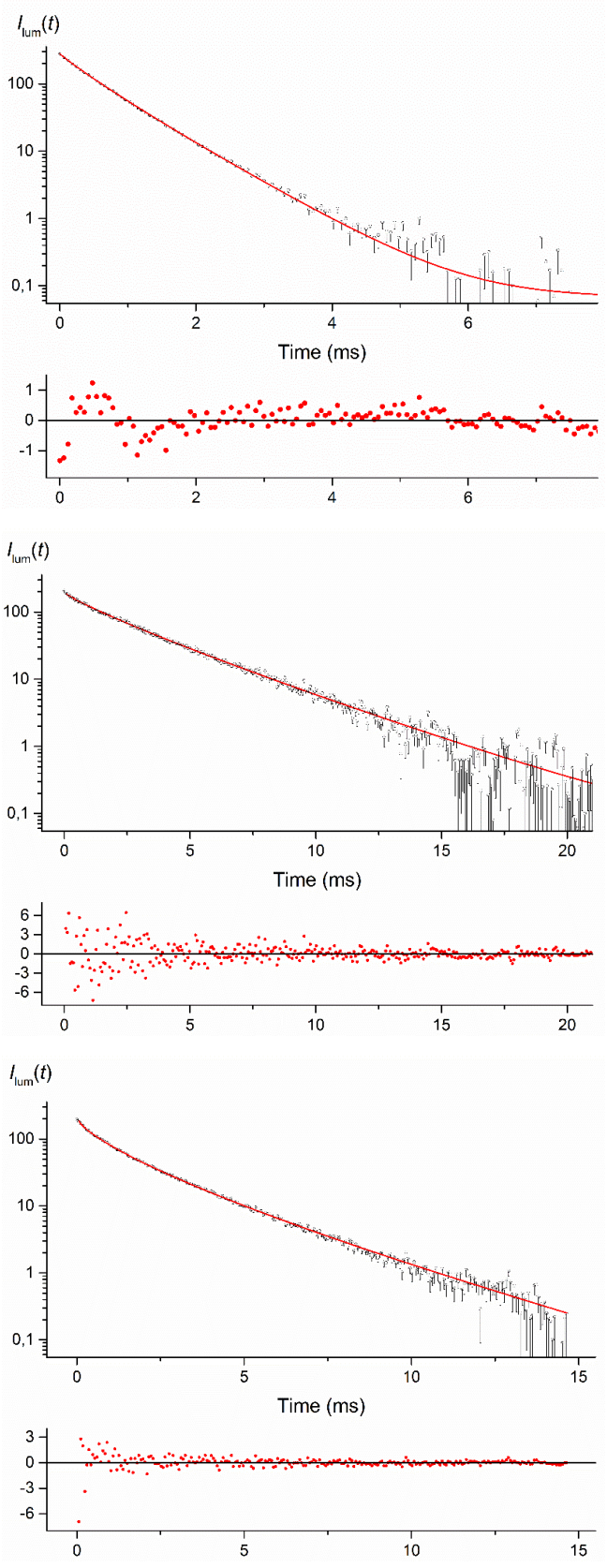

FIG. 6. Luminescence intensity decay of europium ions for nanoparticles: a – ZrO_2:1 mol.% Eu^{3+} annealed at 1200 °C; b – ZrO_2:1 mol.% Eu^{3+}; c – ZrO_2:10 mol.% Eu^{3+}

References

[1] Eichler J., Eisele U., Rodel J. Mechanical properties of monoclinic zirconia. *J. Am. Ceram. Soc.*, 2004, **87** (7), P. 1401–1403.

[2] Aktasa B., Tekelib S., Salman S. Improvements in microstructural and mechanical properties of ZrO_2 ceramics after addition of BaO. *Ceramics International*, 2016, **42**, P. 3849–3854.

[3] Borik M.A., Bublik V.T., Vilkova M.Yu., et al. Structure, phase composition and mechanical properties of ZrO_2 partially stabilized with Y_2O_3. *Modern Electronic Materials*, 2015, **1** (1), P. 26–31.

[4] Lyapunova E.A., Uvarov S.V., Grigoriev M.V., et al. Modification of the mechanical properties of zirconium dioxide ceramics by means of multiwalled carbon nanotubes. *Nanosystems: physics, chemistry and mathematics*, 2016, **7** (1), P. 198–203.

[5] Ramachandra M., Abhishek A., Siddeshwar P., Bharathi V. Hardness and wear resistance of ZrO_2 nanoparticle reinforced Al nanocomposites produced by powder metallurgy. *Procedia Materials Science*, 2015, **10**, P. 212–219.

[6] Grathwohl G., Liu T. Crack resistance and fatigue of transforming ceramics: II, CeOs-stabilized tetragonal ZrO_2. *J Am. Ceram. Soc.*, 1991, **74** (12), P. 3028–3034.

[7] Hayashi H., Saitou T., Maruyama N., et al. Thermal expansion coefficient of yttria-stabilized zirconia for various yttria contents. *Solid State Ionics*, 2005, **176** (5–6), P. 613–619.

[8] Leclercq B., Mevrel R., Liedtke V., Hohenauer. W. Thermal conductivity of zirconia-based ceramics for thermal barrier coating. *Hohenauer Mat.-wiss. u. Werkstofftech*, 2003, **34**, P. 406–409.

[9] Bugrov A.N., Rodionov I.A., Smyslov R.Yu., et al. Photocatalytic activity and luminescent properties of Y, Eu, Tb, Sm and Er-doped ZrO_2 nanoparticles obtained by hydrothermal method. *Int. J. Nanotechnology*, 2016, **13** (1/2/3), P. 147–157.

[10] Klimke J., Trunec M., Krell A. Transparent tetragonal yttria-stabilized zirconia ceramics: influence of scattering caused by birefringence. *J. Am. Ceram. Soc.*, 2011, **94** (6), P.1850–1858.

[11] Shojai F., Mantyla T.A. Chemical stability of yttria-doped zirconia membranes in acid and basic aqueous solutions: chemical properties, effect of annealing and aging time. *Ceramics International*, 2001, 27 (3), P. 299–307.

[12] Reisfeld R., Zelner M., Patra A. Fluorescence study of zirconia films doped by Eu, Tb and Sm and their comparison with silica films. *Journal of Alloys and Compounds*, 2000, **300–301**, P. 147–151.

[13] Jerman M., Qiao Z., Mergel D. Refractive index of thin films of SiO_2, ZrO_2, and HfO_2 as a function of the films mass density. *Applied Optics*, 2005, **44** (15), P. 3006–3012.

[14] Soares M.R.N., Nico C., Peres M., et al. Structural and optical properties of europium doped zirconia single crystals fibers grown by laser floating zone. *Journal pf Applied Physics*, 2011, **109** (1), P. 013516.

[15] Sinhamahapatra A., Jeon J.-P., Kang J., et al. Oxygen-deficient zirconia (ZrO_{2-x}): A new material for solar light absorption. *Sci. Rep.*, 2016, **6**, P. 27218.

[16] Chen X., Liu Y., Tu D. *Lanthanide-doped luminescent nanomaterials: from fundamentals to bioapplications*. Springer-Verlag Berlin Heidelberg, 2014, 208 p.

[17] Stefanic G., Music S. Factors influencing the stability of low temperature tetragonal ZrO_2. *Croatica Chemica Acta*, 2002, **75** (3), P. 727–767.

[18] Vasilevskaya A., Almjasheva O.V., Gusarov V.V. Peculiarities of structural transformations in zirconia nanocrystals. *Journal of Nanoparticle Research*, 2016, **18** (188), 11 p.

[19] Kurapova O.Yu., Konakov V.G. Phase evolution in zirconia-based systems. *Rev. Adv. Mater. Sci*., 2014, **36**, P. 177–190.

[20] Sahina O., Demirkola H., Gocmez M., et al. Mechanical properties of nanocrystalline tetragonal zirconia stabilized with CaO, MgO and Y_2O_3. *Acta Physica Physica Polonica A*, 2013, **123** (2), P. 296–298.

[21] Romer V.H., Rosa E., Lopez-Luke T., et al. Brilliant blue, green and orange-red emission band on Tm^{3+}-, Tb^{3+}- and Eu^{3+}-doped ZrO_2 nanocrystals. *Journal of Physics D: Applied Physics*, 2010, 43, P. 465105.

[22] Almjasheva O.V., Smirnov A.V., Fedorov B.A., et al. Structural features of ZrO_2–Y_2O_3 and ZrO_2–Gd_2O_3 nanoparticles formed under hydrothermal conditions. *Russian Journal of General Chemistry*, 2014, **84** (5), P. 804–809.

[23] Almjasheva O.V., Garabadzhiu A.V., Kozina Yu.V., et al. Biological effect of zirconium dioxide-based nanoparticles. *Nanosystems: physics, chemistry and mathematics*, 2017, **8** (3), P. 391–396.

[24] Fabris S. A stabilization mechanism of zirconia based on oxygen vacancies only. *Acta Mater*., 2002, **50**, P. 5171–5178.

[25] Smits K., Grigorjeva L., Millers D., et al. Europium doped zirconia luminescence. *Opt. Mater. (Amst)*, 2010, **32**, P. 827–831.

[26] Meetei S.D., Singh S.D. Hydrothermal synthesis and white light emission of cubic ZrO_2:Eu^{3+} nanocrystals. *Journal of Alloys and Compounds*, 2014, **587**, P. 143–147.

[27] Smits K., Olsteins D., Zolotarjovs A., et al. Doped zirconia phase and luminescence dependence on the nature of charge compensation. *Scientific Reports*, 2017, **7**, P. 444–453.

[28] Tiseanu C., Cojocaru B., Parvulescu V.I., et al. Order and disorder effects in nano-ZrO_2 investigated by micro-Raman and spectrally and temporarily resolved photoluminescence. *Phys. Chem. Chem. Phys.*, 2012, **14**, P. 12970–12981.

[29] Liu Y., Tu D., Zhu H., Chen X. Lanthanide-doped luminescent nanoprobes: controlled synthesis, optical spectroscopy, and bioapplications. *Chem. Soc. Rev.*, 2013, **42**, P. 6924–6958.

[30] Gupta S.K., Natarajan V. Synthesis, characterization and photoluminescence spectroscopy of lanthanide ion doped oxide materials. *BARC Newsletter*, 2015, P. 14–21.

[31] Bugrov A.N., Zavialova A.Yu., Smyslov R.Yu., et al. Luminescence of Eu^{3+} ions in hybrid polymer-inorganic composites based on poly(methyl methacrylate) and zirconia nanoparticles. *Luminescence*, 2018, P. 1–13.

[32] Mon A., Ram S. Enhanced phase stability and photoluminescence of Eu^{3+} modified t-ZrO_2 nanoparticles. *J. Am. Ceram. Soc.*, 2008, **91** (1), P. 329–332.

[33] Vidya Y.S., Anantharaju K.S., Nagabhushana H., et al. Combustion synthesized tetragonal ZrO_2:Eu^{3+} nanophosphors: Structural and photoluminescence studies. *Spectrochimica Acta Part A: Molecular and Biomolecular Spectroscopy*, 2015, **135**, P. 241–251.

[34] Ghosh P., Patra A. Role of surface coating in ZrO_2/Eu^{3+} nanocrystals. *Langmuir*, 2006, **22**, P. 6321–6327.

[35] Ninjbadgar T., Garnweitner G., Borger A., et al. Synthesis of luminescent ZrO_2:Eu^{3+} nanoparticles and their holographic sub-micrometer patterning in polymer composites. *Adv. Funct. Mater.*, 2009, **19**, P. 1819–1825.

[36] Hobbs H., Briddon S., Lester E. The synthesis and fluorescent properties of nanoparticulate ZrO_2 doped with Eu using continuous hydrothermal synthesis. *Green Chem.*, 2009, **11**, P. 484–491.
[37] Lopato L.M., Andrievskaya E.R., Shevchenko A.V., Red'ko V.P. Phase relations in the ZrO_2–Eu_2O_3 system. *Russian Journal of Inorganic Chemistry*, 1997, **42** (10), P. 1588–1591.
[38] Bugrov A.N., Almjasheva O.V. Effect of hydrothermal synthesis conditions on the morpholgy of ZrO_2 nanoparticles. *Nanosystems: physics, chemistry and mathematics*, 2013, **4** (6), P. 810–815.
[39] Bortolotti M., Lutterotti L., Lonardelli I. ReX: a computer program for structural analysis using powder diffraction data. *J. Appl. Cryst.*, 2009, **42** (3), P. 538–539.
[40] Vasilef I. *QTIPLOT, Data Analysis and Scientific Visualisation*. Universiteit Utrecht, Utrecht, Niederlande, 2011.
[41] Smith D.K., Newkirk H.W. The crystal structure of baddeleyite (monoclinic ZrO_2) and its relation to the polymorphism of ZrO_2. *Acta Crystallographica*, 1965, **18**, P. 983–991.
[42] Igawa N., Ishii Y. Crystal structure of metastable tetragonal zirconia up to 1473 K. *J. Am. Ceram. Soc.*, 2001, **84** (5), P. 1169–1171.
[43] Martin U., Boysen H., Frey F. Neutron powder investigation of tetragonal and cubic stabilized zirconia, TZP and CSZ, at temperatures up to 1400 K. *Acta Crystallographica Section B*, 1993, **49** (3), P. 403–413.
[44] Meetei S.D., Singh S.D., Singh N.S., et al. Crystal structure and photoluminescence correlations in white emitting nanocrystalline ZrO_2:Eu^{3+} phosphor: Effect of doping and annealing. *Journal of Luminescence*, 2012, **132**, P. 537–544.
[45] Basahel S.N., Ali T.T., Mokhtar M., Narasimharao K. Influence of crystal structure of nanosized ZrO_2 on photocatalytic degradation of methyl orange. *Nanoscale Research Letters*, 2015, **10** (73), 13 p.
[46] Adamski A., Jakubus P., Sojka Z. Synthesis of nanostructured tetragonal ZrO_2 of enhanced thermal stability. *Nukleunika*, 2006, **51**, P. 27–33.
[47] Bersani D., Lottici P.P., Rangel G., et al. Micro-Raman study of indium doped zirconia obtained by sol-gel. *J Non-Crystalline Solids*, 2004, **345–346**, P. 116–119.
[48] Gazzoli D., Mattei G., Valigi M. Raman and X-ray investigations of the incorporation of Ca^{2+} and Cd^{2+} in the ZrO_2 structure. *J Raman Spectrosc.*, 2007, **38** (7), P. 824–831.
[49] Kerbellec N., Catala L., Daiguebonne C., et al. Luminescent coordination nanoparticles. *New J. Chem.*, 2008, **32**, P. 584–587.
[50] Lakowicz J. *Principles of Fluorescence Spectroscopy*, 3rd ed. Springer, New York, 2006.
[51] Ishida H., Bunzli J.-C., Beeby A. Guidelines for measurement of luminescence spectra and quantum yields of inorganic and organometallic compounds in solution and solid state (IUPAC Technical Report). *Pure Appl. Chem.*, 2016, **88** (7), P. 701–711.
[52] Novikov E.G., Hoek A., Visser A., Hofstraat J.W. Linear algorithms for stretched exponential decay analysis. *Optics Communications*, 1999, **166**, P. 189–198.
[53] Klatt J., Gerich C., Grobe A., et al. Fractal dimension of time-resolved autofluorescence discriminates tumour from healthy tissues in the oral cavity. *Journal of Cranio-Maxillo-Facial Surgery*, 2014, **42** (6), P. 852-854.
[54] Lianos P., Duportail G. Time-resolved fluorescence fractal analysis in lipid aggregates. *Biophys. Chem.*, 1993, **48**, P. 293–299.